J Solid State Electrochem (2012) 16:829–834
DOI 10.1007/s10008-011-1437-1

REVIEW

May 3D nickel foam electrode be the promising choice for supercapacitors?

You-Ling Wang · Yong-Qing Zhao · Cai-Ling Xu

Received: 25 February 2011 / Revised: 15 May 2011 / Accepted: 17 May 2011 / Published online: 3 June 2011

Abstract The manganese oxide (MnO_2) nanowires and cobalt hydroxide ($Co(OH)_2$) nanosheets are successfully electrodeposited on nickel foam (NF), respectively (referred to as MnO_2/NF and $Co(OH)_2$/NF electrode hereinafter). Both electrodes show higher specific capacitance (C_s) and more excellent rate performance than that of most reported corresponding materials. In addition, our previous study of $Ni(OH)_2$/NF electrodes also exhibited conspicuous results. Combined with the outstanding properties of NF, it is noticeable that the NF electrodes may be a promising choice for supercapacitors.

Keywords Supercapacitor · Electrodeposition · Nickel foam · Manganese oxide · Cobalt hydroxide

Introduction

Over the past decades, supercapacitors have been paid great attention owing to their higher power density and longer life cycle than secondary batteries, and higher energy density compared with conventional electrical double-layer capacitors [1–4]. Although supercapacitors are one of the most promising candidates in the electric vehicle applications, it is highly desirable to enhance the energy density of supercapacitors to approach that of batteries, which could enable their use as primary power sources [5, 6]. To obtain advanced supercapacitors, the improvement of electrode performance is requisite. In recent years, tremendous efforts have been made to discover new materials and optimize the properties of the electrode material itself [7]. Among them, nanomaterials have attracted great attention as they present higher specific capacitance (C_s) and better rate capability compared with traditional bulk materials [8]. On the other hand, many efforts have also been devoted to reforming the traditional electrode structure [5, 9, 10]. Generally, there are mainly two approaches for preparing electrodes. One case is powder-based electrodes which are fabricated by pressing the mixed slurry of the electroactive material, conductivity enhancer, and binder on the current collector [11]. However, the use of binder and/or other adhesive not only reduces the energy density but also introduces extra contact resistance between electronic conductors and active materials leading to lower power density. Moreover, the preparation processes are complicated. The other case is the thin film electrodes which are prepared by directly depositing active materials onto the conductive substrates (such as carbon nanotube papers [12], stainless-steel collectors, nickel foils [13], etc.), whereas, it is reported that the performance of the electrode would fade with the increasing of film thickness because the inner active material is not really accessible [14]. Recently, a novel three-dimensional (3D), porous, hierarchical electrode structure has attracted more interests. This architecture possesses larger specific area, can significantly reduce the diffusion length of ions and greatly enhance the ionic conductivity and electronic conductivity. Typically, Hu et al. fabricated 3D $RuO_2 \cdot xH_2O$ nanotube array electrode by means of electrodeposition technique and anodic alumi-

Y.-L. Wang · Y.-Q. Zhao (✉) · C.-L. Xu (✉)
Key Laboratory of Nonferrous Metal Chemistry and Resources Utilization of Gansu Province, School of Chemistry and Chemical Engineering, Lanzhou University,
Lanzhou 730000, China
e-mail: yqzhao@lzu.edu.cn

C.-L. Xu
e-mail: xucl@lzu.edu.cn

num oxide templates, which exhibited ultrahigh-power characteristics and high capacitance [5]. Cao et al. prepared manganese oxide nanoflower/carbon nanotube array composite electrodes by combining electrodeposition technique and chemical vapor deposition method. This electrode presented excellent rate capability, high capacitance, and long cycle life, with a strong promise for high-rate electrochemical capacitive energy storage applications [10]. However, the complexity and high cost of the above methods will greatly impede its practical application. Consequently, the development of a 3D cost-effective electrode fabricated by a facile process is necessary for supercapacitor applications.

Nickel foam (NF), as a cheap commercial material, is widely used as support for electrode material due to its high electronic conductivity, desirable 3D open-pore structure, and high specific surface area. However, designing a 3D electrode structure from nickel foam as host was never given more attention until our group showed the excellent performance of the $Ni(OH)_2$/NF electrode which was simply designed by directly electrodepositing $Ni(OH)_2$ on the NF [9]. This electrode also has a 3D porous hierarchical structure and the corresponding merits. Furthermore, it has a lower cost and can be easily fabricated. Thus, the NF may be a promising candidate for designing an advanced electrode structure for energy storage/conversion devices.

In this communication, the manganese oxide (MnO_2)/NF and cobalt hydroxide ($Co(OH)_2$)/NF electrodes were constructed for certifying the reliability and superiority of the NF electrodes. A maximum C_s of 691 Fg^{-1} at 5 Ag^{-1} for the MnO_2/NF electrode was obtained, and it also presented superb rate performance (330 Fg^{-1}, 47.8% capacitance retention at 100 Ag^{-1}). The $Co(OH)_2$/NF electrode achieved the maximum C_s of 3,255 Fg^{-1} at 5 Ag^{-1}, and had 73.1% capacitance retention at 60 Ag^{-1}. The high C_s and excellent rate performance of the two electrodes demonstrate that NF electrodes may be a promising choice for high-rate electrochemical capacitive energy storage applications.

Experimental

NF (thickness, 1.8 mm; pore density, 110 ppi) was used as the support and current collector of MnO_2 and $Co(OH)_2$. Before the electrodeposition, NF was rinsed with acetone and hydrochloric acid to clean and etch the metal surface, respectively. The electrodeposition was conducted on the CHI660b model electrochemical workstation, with a three-electrode cell consisting of a saturated calomel electrode (SCE) as reference electrode, a 3.0×3.0-cm platinum plate as counter electrode and the treated NF as the working electrode. For the MnO_2/NF electrode, the electrodeposition experiment was carried out at a constant potential of 1.0 V vs. SCE in the aqueous solution of 0.5 M $Mn(CH_3COO)_2$, and the MnO_2 mass load was 0.06 mg cm^{-2}. For the $Co(OH)_2$/NF electrode, the electrodeposition experiment was carried out at a constant potential of −0.75 vs. SCE in the aqueous solution of 0.9 M $Co(NO_3)_2$ and 0.075 M $NaNO_3$, and the $Co(OH)_2$ mass load was 0.5 mg cm^{-2}. After deposition, the as-prepared MnO_2/NF and $Co(OH)_2$/NF electrodes were washed several times by distilled water, then were heat-treated at 200 and 120 °C for 2 h, respectively [15]. The mass of MnO_2 and $Co(OH)_2$ were calculated by Faraday's law on the basis of the coulombic charge passed during electrolysis.

All electrochemical measurements were carried out in a conventional three-electrode cell on a CHI660b electrochemical workstation. The cell consisted of the a MnO_2/NF electrode or $Co(OH)_2$/NF electrode as the working electrode, a Pt foil of 3.0×3.0 cm as the counter electrode, SCE the as reference electrode for MnO_2/NF, and Hg/HgO/5.5 M KOH (MMO) as the reference electrode for $Co(OH)_2$/NF. The electrolyte was an aqueous solution of 0.5 M Na_2SO_4 for MnO_2/NF electrode and 5.5 M KOH for the $Co(OH)_2$/NF electrode.

The C_s was measured by chronopotentiometry and calculated according to the equation:

$$C_s = I \times \Delta t / \Delta V \times m \quad (1)$$

where C_s (farad per gram) is the specific capacitance of the electrode, I (ampere) is the constant discharging current, Δt (seconds) is the discharging time, ΔV (volts) is the potential drop at a constant discharge current, and m (grams) is the mass of the active materials measured. The morphology of the electrodeposited MnO_2 and $Co(OH)_2$ layer was characterized using a field emission scanning electron microscope (FESEM, JEOL JSM-S4800). X-ray diffraction (XRD) data were collected using a Rigaku D/MAX 2400 diffractometer (Japan) with a Cu Kα radiation (k=1.5418 Å) operating at 40.0 kV, 60.0 mA.

Results and discussion

The surface morphology and microstructure of the treated NF, MnO_2/NF, and $Co(OH)_2$/NF electrodes are schematically shown in Fig. 1. It can be seen that the NF has 3D porous and cross-linked grid structure (Fig. 1a). A close examination reveals that there are considerable uniform wrinkles on its surface with highly porous structures (Fig. 1b). MnO_2 deposited on the surface of

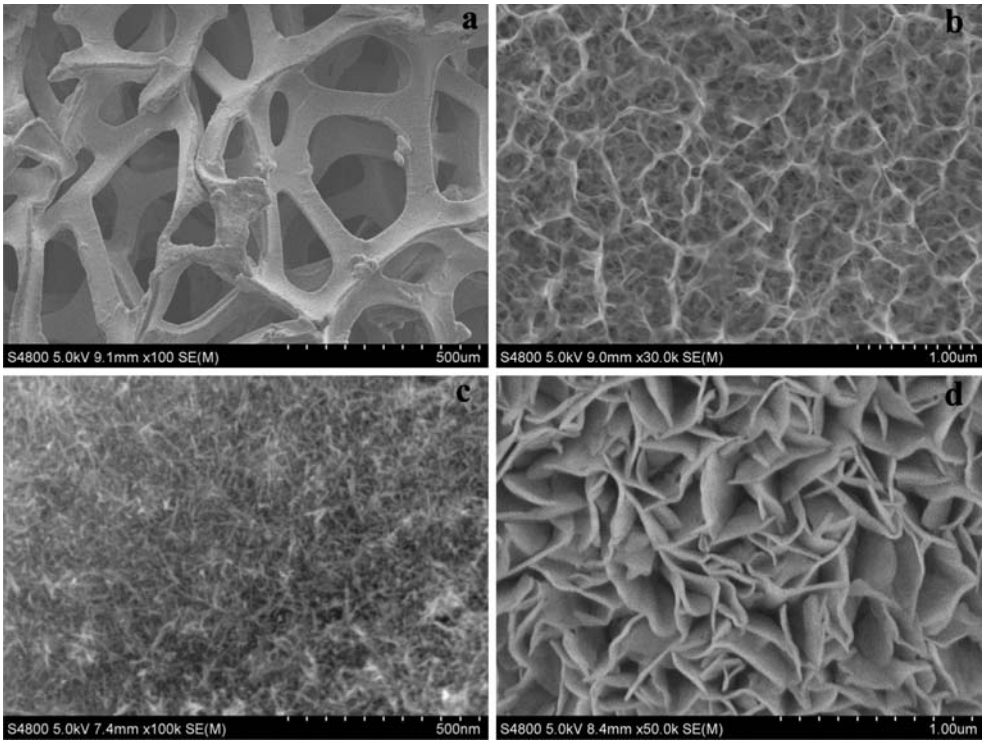

Fig. 1 FESEM micrographs of an overview of NF (**a**). An enlarged view for the surface of NF (**b**); MnO_2 coating (**c**) and $Co(OH)_2$ coating (**d**) on the surface of NF

NF exhibits nanowire structure with higher porosity than nanoparticle structure (Fig. 1c). The $Co(OH)_2$/NF electrode displays interlaced nanosheet-like characteristic, suggesting the high surface area (Fig. 1d). The structure of the MnO_2/NF and $Co(OH)_2$/NF electrodes is beneficial for providing a more active area for charge storage and delivery and facilitating the diffusion of ions, thus may generate high capacitance.

Figure 2 illustrates the X-ray diffraction patterns of the as-prepared MnO_2 and $Co(OH)_2$ materials. As is seen from Fig. 2a, the main characteristic peaks of the α-MnO_2 can be roughly identified, and the broad and low intense peaks confirm the amorphous nature of MnO_2, which is in agreement with the previous works [15–17]. Figure 2b presents the XRD pattern of the $Co(OH)_2$. It can be observed that all peaks are in good agreement with the patterns of β-$Co(OH)_2$ (JCPDS no. 30–0443). The main peaks of $Co(OH)_2$ are labeled with hkl indexes.

The cyclic voltammetry curves (CVs) of the MnO_2/NF and $Co(OH)_2$/NF electrodes are presented in Fig. 3. The CV curves of the bare NF electrode were also recorded under the same condition. The result showed that the capacitive contribution of NF is negligible compared with MnO_2 electrodes. Figure 3a exhibits the CVs of the MnO_2/NF electrode at various scan rates. Rectangular and symmetric images of the CVs at low scan rate are observed between −0.1 and +0.9 V, indicating high electrochemical reversibility of the MnO_2/NF electrode. Even the scan rate up to 700 mV s^{-1}, there is only slight distortion from the ideal symmetrical rectangle shape, which strongly shows a good rate capability of the electrodes.

Figure 3b displays the CVs of the $Co(OH)_2$/NF electrode at various scan rates. As is seen, two pairs of redox peaks are visible. According to the literatures, two plausible reactions could occur as quasireversible redox processes during the potential sweep of the electrode [6, 18]:

$$Co(OH)_2 + OH^- \underset{\text{discharge}}{\overset{\text{charge}}{\rightleftharpoons}} CoOOH + H_2O + e^- \qquad (2)$$

$$CoOOH + OH^- \underset{\text{discharge}}{\overset{\text{charge}}{\rightleftharpoons}} CoO_2 + H_2O + e^- \qquad (3)$$

The anodic peak P_1 is ascribed to the oxidation of $Co(OH)_2$ to CoOOH, and the cathodic peak P_2 is for the reverse process. The anodic peak P_3 is assigned to the oxidation of CoOOH to CoO_2, and the cathodic peak P_4 is for the reverse process. With the increase of the scan rates, the characteristic CV shapes of the $Co(OH)_2$/NF electrode are not significantly affected, which also shows good rate capability.

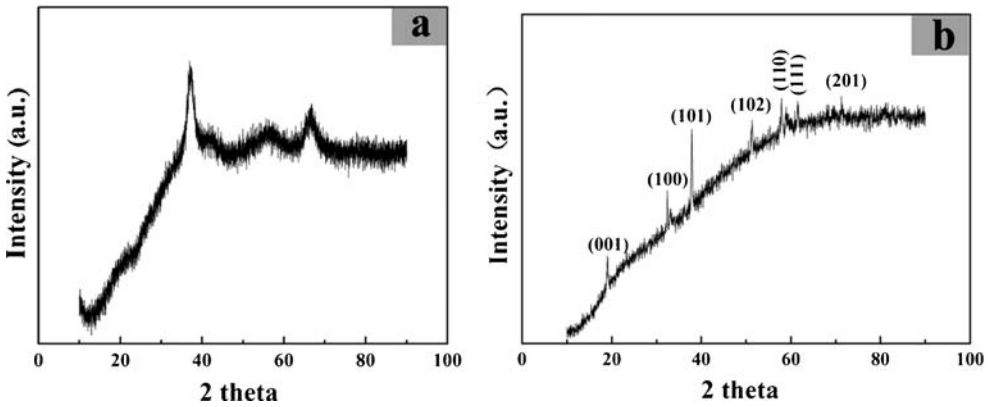

Fig. 2 XRD patterns of MnO_2 (**a**) and $Co(OH)_2$ (**b**)

The CV results reveal that both the MnO_2/NF and $Co(OH)_2$/NF electrodes have excellent power properties. It is probably due to the 3D open-pore structure and good conductivity of NF, which provide more active area and highways for charge storage and delivery. Additionally, the nanosized porous structure of MnO_2 and $Co(OH)_2$ could ensure enough ions to contact the active materials in a short time and a high utilization of electrode materials, thus lead to the excellent capacitance behavior and rate capability.

To further investigate the capacitive performance of MnO_2/NF and $Co(OH)_2$/NF electrodes, galvanostatic charge/discharge over the range of −0.1 to +0.9 V and −0.05 to +0.5 V were recorded, respectively. Typically, Fig. 4a shows the chronopotentiograms of the MnO_2/NF electrode at a charge–discharge current density of 5 Ag^{-1} in 0.5 M Na_2SO_4 aqueous solution. It is noted that the curve for the MnO_2/NF electrode is highly linear and symmetrical. The C_s calculated from Fig. 4a is 691 Fg^{-1}, which is higher than many reported values. The C_s of the powder-based electrodes for MnO_2 is usually in the range of 200–400 Fg^{-1}, which seriously limits their further commercial applications [2, 19, 20]. Furthermore, compared with the reported thin film electrodes that the MnO_2 were directly deposited on other conducting substrates, the MnO_2/NF electrode also exhibits superior C_s. For example, it is only 167.5 Fg^{-1} for the CNT paper at a current density of 77 mA g^{-1} [12], 230 Fg^{-1} for the Pt foil substrate at the scan rate 20 mV s^{-1} [21], 240 Fg^{-1} for the Ni sheet at the current density of 1 mA cm^{-2} [8], and 460 Fg^{-1} for the Ti foil substrate at the scan rate 10 mV s^{-1} [22]. It is obvious that NF as conducting substrate is an ideal choice for MnO_2 supercapacitors.

The relationship between the C_s and charge/discharge current density is also investigated. Figure 4b plots the variation of the C_s values with charge/discharge current density for the MnO_2/NF electrode. As expected, the C_s decreases with the increasing charge/discharge current density. Based on the C_s obtained at 5 Ag^{-1}, the electrode has the capacitance retention of 47.8% (330 Fg^{-1}) at 100 Ag^{-1}, which is much higher than most reported values obtained at low current densities or low scan rates [8, 12, 21, 22]. The

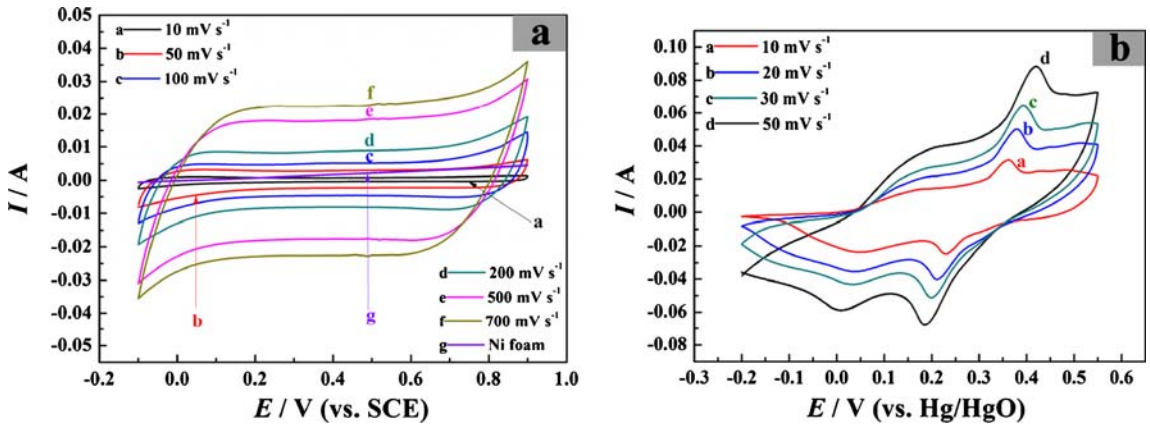

Fig. 3 CV curves at different scan rates for the MnO_2/NF (**a**) and $Co(OH)_2$/NF (**b**) electrode

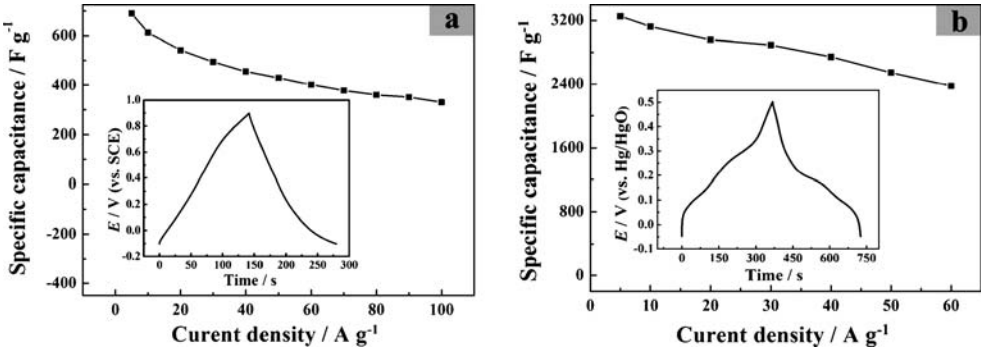

Fig. 4 Charge/discharge curves at 5 Ag^{-1} and specific capacitance as a function of the discharge current density for MnO_2/NF (**a**) and $Co(OH)_2$/NF (**b**)

excellent rate capability is consistent with the result of the CVs.

Figure 4c presents the chronopotentiograms of $Co(OH)_2$/NF electrode at 5 Ag^{-1} in 5.5 M KOH aqueous solution and the corresponding C_s is 3,254.5 Fg^{-1} in the potential range of −0.05 to 0.5 V. From the shape of the charge/discharge curve, it can be known that the electrode mainly exhibits a pseudocapacitance characteristic rather than the pure double-layer capacitor, which can also be observed from the shape of the CVs. Figure 4d shows that the Co $(OH)_2$/NF electrode also exhibits excellent rate capability. Based on the capacitance at 5 Ag^{-1}, the capacitance retention remains 73.1% (2,378.1 Fg^{-1}) at 60 Ag^{-1}. The results of the $Co(OH)_2$/NF electrode are also much superior to that of reported $Co(OH)_2$ materials [23–26]. Furthermore, similar to the MnO_2/NF electrode, the C_s also decreases with the increasing charge/discharge current density. The phenomenon is due to the increasing of potential drop and the relatively insufficient Faradic redox reaction of the electrode materials under higher discharge current densities [27].

In order to evaluate the electrochemical stability of the MnO_2/NF and $Co(OH)_2$/NF electrodes, the charge–discharge cycling were carried out in 0.5 M Na_2SO_4 and 5.5 M KOH aqueous solution at the current density of 5 A g^{-1}, respectively. From Fig. 5a, b, it can be observed that the cycling performances of the two electrodes are similar to the reported $Ni(OH)_2$-NF electrode. Within the first 150 cycles, the repetitive charge/discharge led to noticeable discharge specific capacitance losses for both electrodes. From the 150th cycle, the reduction of specific capacitance with cycle number becomes lower. After 300 cycles, the MnO_2/NF and $Co(OH)_2$/NF electrodes only retained 28% (196 Fg^{-1}) and 34% (1,099 Fg^{-1}) of their initial capacitances, respectively. However, taking account of the attractive specific capacitance and rate capability exhibited by these electrodes, NF electrodes may be potential electrodes for high-power supercapacitors if their cycling performance can be effectively enhanced.

Conclusions

In summary, the MnO_2/NF electrode and $Co(OH)_2$/NF electrode were simply fabricated by direct electrochemical deposition method. Both electrodes showed higher C_s and more excellent rate performance than that of most reported corresponding materials. Besides, the $Ni(OH)_2$/NF electrode also has been highlighted due to its higher C_s [9]. Therefore, it can be believed that the NF electrode is reliable and superb, and thus it may be a promising choice for supercapacitors.

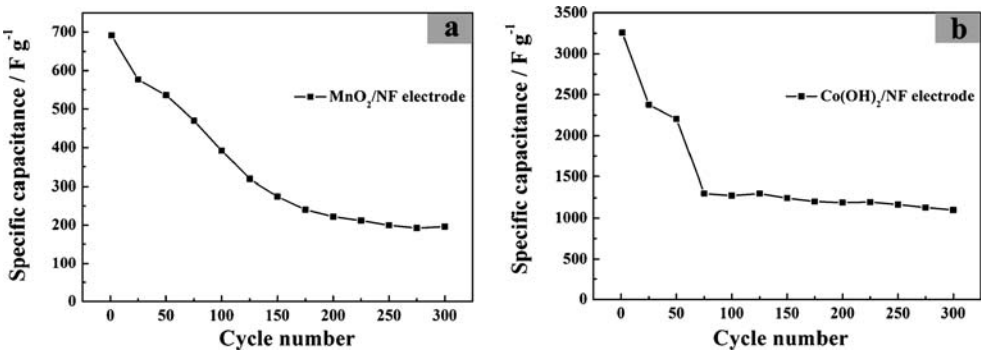

Fig. 5 Charge/discharge cycling test for the MnO_2/NF (**a**) and $Co(OH)_2$/NF (**b**) electrode at the current density of 5 Ag^{-1}

Acknowledgments This work was supported by grants from the Natural Science Foundation of China (NNSFC no. 20903050), the Fundamental Research Funds for the Central University (Lzujbky-2009-28), the China Postdoctoral Science Foundation (20070420133).

References

1. Choi D, Blomgren GE, Kumta PN (2006) Adv Mater 18:1178–1182
2. Xu M-W, Wei J, Bao S-J, Su Z, Dong B (2010) Electrochim Acta 55:5117–5122
3. Nam K-W, Lee C-W, Yang X-Q, Cho BW, Yoon W-S, Kim K-B (2009) J Power Sources 188:323–331
4. Kim C, Ngoc BTN, Yang KS, Kojima M, Kim YA, Kim YJ, Endo M, Yang SC (2007) Adv Mater 19:2341–2346
5. Hu C-C, Chang K-H, Lin M-C, Wu Y-T (2006) Nano Lett 6:2690–2695
6. Cao L, Xu F, Liang Y-Y, Li H-L (2004) Adv Mater 16:1853–1857
7. Chen S, Zhu J, Wu X, Han Q, Wang X (2010) ACS Nano 4:2822–2830
8. Chou S, Cheng F, Chen J (2006) J Power Sources 162:727–734
9. Yang G-W, Xu C-L, Li H-L (2008) Chem Commun 6537–6539
10. Zhang H, Cao G, Wang Z, Yang Y, Shi Z, Gu Z (2008) Nano Lett 8:2664–2668
11. Yuan AB, Wang ML, Wang YQ, Hu J (2009) Electrochim Acta 54:1021–1026
12. Chou S-L, Wang J-Z, Chew S-Y, Liu H-K, Dou S-X (2008) Electrochem Commun 10:1724–1727
13. Pang S-C, Anderson MA, Chapman TW (2000) J Electrochem Soc 147:444–450
14. Li J, Yang QM, Zhitomirsky I (2008) J Power Sources 185:1569–1574
15. Xu C-L, Bao S-J, Kong L-B, Li H, Li H-L (2006) J Solid State Chem 179:1351–1355
16. Toupin M, Brousse T, Belanger D (2004) Chem Mater 16:3184–3190
17. Xu C, Zhao Y, Yang G, Li F, Li H (2009) Chem Commun 7575–7577
18. Zhou W-J, Xu M-W, Zhao D-D, Xu C-L, Li H-L (2009) Microporous Mesoporous Mater 117:55–60
19. Yu P, Zhang X, Chen Y, Ma Y, Qi Z (2009) Mat Chem Phys 118:303–307
20. Tang X, Liu Z-H, Zhang C, Yang Z, Wang Z (2009) J Power Sources 193:939–943
21. Xia H, Xiao W, Lai MO, Lu L (2009) Nanoscale Res Lett 4:1035–1040
22. Dong B, Xue T, Xu C-L, Li H-L (2008) Microporous Mesoporous Mater 112:627–631
23. Kong L-B, Lang J-W, Liu M, Luo Y-C, Kang L (2009) J Power Sources 194:1194–1201
24. Liang Y-Y, Cao L, Kong L-B, Li H-L (2004) J Power Sources 136:197–200
25. Tao F, Shen Y, Liang Y, Li H (2007) J Solid State Electrochem 11:853–858
26. Gupta V, Kusahara T, Toyama H, Gupta S, Miura N (2007) Electrochem Commun 9:2315–2319
27. Qu Q, Zhang P, Wang B, Chen Y, Tian S, Wu Y, Holze R (2009) J Physical Chemistry C 113:14020–14027